Model Predictive Control Methods to Reduce Common-Mode Voltage for Three-Phase Voltage Source Inverters

Sangshin Kwak, *Member, IEEE*, and Sung-ki Mun

***Abstract*—In this paper, we propose model predictive control methods to reduce the common-mode voltage of three-phase voltage source inverters (VSIs). In the reduced common-mode voltage-model predictive control (RCMV-MPC) methods proposed in this paper, only nonzero voltage vectors are utilized to reduce the common-mode voltage as well as to control the load currents. In addition, two nonzero voltage vectors are selected from the cost function at every sampling period, instead of using only one optimal vector during one sampling period. The two selected nonzero vectors are distributed in one sampling period in such a way as to minimize the error between the measured load current and the reference. Without utilizing the zero vectors, the common-mode voltage controlled by the proposed RCMV-MPC algorithms can be restricted within $\pm V_{\rm dc}/6$. Furthermore, application of the two nonzero vectors with optimal time sharing between them can yield satisfactory load current ripple performance without using the zero vectors. Thus, the proposed RCMV-MPC methods can reduce the common-mode voltage as well as control the load currents with fast transient response and satisfactory load current ripple performance compared with the conventional model predictive control method. Simulation and experimental results are included to verify the effectiveness of the proposed RCMV-MPC methods.**

***Index Terms*—Common-mode voltage, current control, predictive control, voltage source inverter (VSI).**

I. Introduction

THREE-PHASE voltage source inverters (VSIs) with proportional-integral (PI) control methods with distinct pulse width modulation (PWM) blocks have been popularly used to provide output currents with controllable amplitude and controllable frequency [1]–[8]. In the VSI, common-mode voltages generated by the fast switching operation have been known to give rise to overvoltage stress to the winding insulation of drives and to conduct or radiate electromagnetic interference, which can affect the functionality of other electronic systems in the vicinity [9]. Several studies have been conducted to reduce the peak common-mode voltage with PWM strategies designed by avoiding the zero vectors because the zero vectors result in the highest common-mode voltages [9]–[11]. The PWM algorithms for reducing the common-mode voltage can be incorporated with the PI current controllers for the VSI not only to reduce the common-mode voltage but also to control the load currents. Recently, a model predictive control method based on a finite-control-set concept has been developed as a simple and effective current control technique for VSIs owing to its simplicity without using any individual PWM blocks as well as its control flexibility [12]–[26]. By using the fundamental principle that only seven different voltage vectors can be applied to the loads by the VSI, the model predictive control method predicts the seven possible future load current behavior patterns of the VSI on the basis of the load dynamic model of the VSI. On the basis of the cost function predefined with error terms between the future load current and the reference, the current controller evaluates all the predicted current values obtained by the seven possible states to select one optimal switching state with the smallest cost value. Finally, the VSI with the model predictive controller applies the optimal switching state during the entire sampling period of the controller. Because of its simplicity with no requirement of individual PWM blocks as well as its control flexibility, the model predictive control scheme has been employed to control the load currents of power converters other than VSIs, such as multilevel inverters, multiphase inverters, active power filters, and matrix converters [14]–[26].

This paper proposes two reduced common-mode voltage-model predictive control (RCMV-MPC) methods to reduce the common-mode voltage of three-phase VSIs on the basis of the model predictive control method. In the proposed RCMV-MPC methods, only six nonzero VSI states are considered to perform model predictive control to reduce the common-mode voltage by avoiding the zero vectors. Furthermore, the proposed methods utilize two nonzero voltage states in one sampling period in order to compensate for the reduced number of voltage states, instead of using only one optimal vector during one sampling period as in the conventional method. The two selected active vectors are distributed within the sampling period in such a way as to minimize the squared current errors between the reference and actual future load currents in the proposed methods. Therefore, the common-mode voltage controlled by the proposed RCMV-MPC algorithms can be restricted within $\pm V_{\rm dc}/6$ without utilizing the zero vectors. Furthermore, applying the two nonzero voltage vectors with optimal time sharing between them can lead to the satisfactory load current ripple performance, despite no utilization of the zero vectors. In one proposed method termed as the RCMV-MPC I in this paper, the two nonzero voltage vectors are simultaneously selected for the purpose of implementing

Manuscript received March 10, 2014; revised August 19, 2014; accepted September 26, 2014. Date of publication October 13, 2014; date of current version April 15, 2015. This work was supported by the National Research Foundation of Korea grant funded by the Korea government (2014R1A2A2A01006684). Recommended for publication by Associate Editor F. W. Fuchs.

The authors are with the School of Electrical and Electronics Engineering, Chung-ang University, 156-756 Seoul, Korea (e-mail: sskwak@ieee.org).

Color versions of one or more of the figures in this paper are available online at http://ieeexplore.ieee.org.

Digital Object Identifier 10.1109/TPEL.2014.2362762

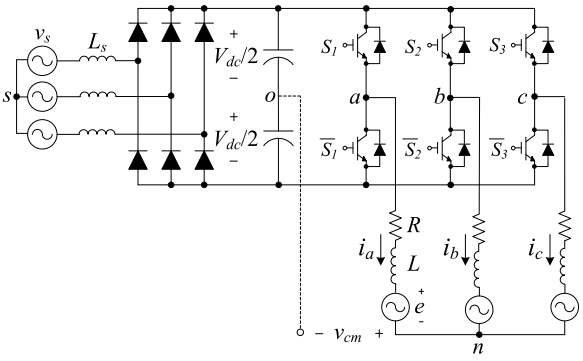

Fig. 1. Three-phase VSI with a diode rectifier.

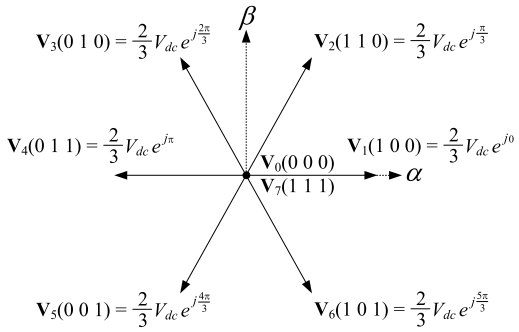

Fig. 2. Voltage vectors generated by the VSI.

without significantly increasing the calculation complexity. In addition to the proposed RCMV-MPC I, this paper also develops a proposed RCMV-MPC II, which in advance selects the first nonzero vector, and then considers the six applicable nonzero voltage vectors as the second nonzero vector. Both the proposed RCMV-MPC methods I and II are compared in terms of the current errors, the total harmonic distortion (THD) values, and the number of switchings in this paper. Based on comparative results, the proposed method II results in better performance in the current errors and the THD values than the proposed method I and the conventional method, at the expense of the increased number of switching and the increased complexity of calculation. In addition, the two proposed RCMV-MPC methods do not affect the fast transient response of the conventional model predictive control method adversely because the zero vectors are not generally selected during transient conditions. Thus, the two proposed RCMV-MPC methods can reduce the common-mode voltage with comparable load current ripple performance without detriment to transient responses, compared with the conventional model predictive control method. A practical consideration to compensate for the unavoidable calculation delay present in the digital signal processor (DSP) is also developed to utilize the two nonzero vectors. Simulation and experimental results are included to verify the effectiveness of the proposed RCMV-MPC methods.

II. Conventional Model Predictive Control Method for VSIs

The three-phase VSI with six insulated gate bipolar transistors (IGBTs) as switches is fed by a diode rectifier and shown in Fig. 1. The voltage vectors applied to the load by the VSI can be expressed in the $\alpha\beta$ frame as

$$v = \frac{2}{3}(v_{an} + v_{bn}e^{j(2\pi/3)} + v_{cn}e^{j(4\pi/3)}) \tag{1}$$

.

Eight voltage vectors including six active and two zero vectors, as shown in Fig. 2, enable the VSI to adjust load currents [12], [13]. The switching functions of the switches take on the binary values "1" and "0" in a closed state and an open state, respectively. The lower switches have the complementary value of their upper switches. Owing to the redundancy of the two zero vectors that generate equal output voltage vectors, only seven control elements are available in the finite control set of the three-phase VSI. The load current can be also described using the space vector definition as

$$i = \frac{2}{3}(i_a + i_b e^{j(2\pi/3)} + i_c e^{j(4\pi/3)}) \tag{2}$$

.

The load current dynamics of the three-phase VSI with a general three-phase resistive-inductive-active (RLe) load is expressed in the space vector form as

$$v = Ri + L\frac{di}{dt} + e \tag{3}$$

where *R*, *L*, and ***e*** are the load resistance, inductance, and back electromotive force (back emf) vector, respectively. The derivative of the load current in the continuous-time model in (3) can be approximated on the basis of the forward Euler approximation with a sampling period T_s as

$$\frac{di}{dt} \approx \frac{i((k+1)T_s) - i(kT_s)}{T_s}. \tag{4}$$

The load current dynamics can be, then, expressed in the discrete-time domain as

$$i((k+1)T_s) = i(kT_s) + \frac{T_s}{L}\left[v^k - Ri(kT_s) - e(kT_s)\right]. \tag{5}$$

Seven voltage vectors of the VSI applied in the *k*th sampling period, $\boldsymbol{v}^k$, generate seven consequent future load current behaviors, which can be predicted on the basis of the load current dynamics in (5). By evaluating each predicted future load current value using a predefined cost function, one optimal voltage vector among seven available voltage vectors is selected to minimize errors between the one-step future reference and real currents in every sampling period. The cost function to measure errors between the references and the predicted load currents in orthogonal coordinates can be defined in terms of the quadratic errors as

$$\begin{aligned} g = {} & \left\{i_\alpha^*\left((k+1)T_s\right) - i_\alpha\left((k+1)T_s\right)\right\}^2 \\ & + \left\{i_\beta^*\left((k+1)T_s\right) - i_\beta\left((k+1)T_s\right)\right\}^2 \end{aligned} \tag{6}$$

where $i_\alpha^*((k+1)T_s)$ and $i_\beta^*((k+1)T_s)$ are the one-step future current values in the $\alpha\beta$ frame. Furthermore, $i_\alpha((k+1)T_s)$ and $i_\beta((k+1)T_s)$ are the components of the predicted load

current in the $\alpha\beta$ coordinate system. Only one optimal voltage vector determined by the cost function is applied during one entire sampling period to force the actual load current vector to approach the reference load current vector at the next step. The future reference current vector required in the cost function can be obtained from the Lagrange extrapolation formula with the present and the two past reference values by [16]

$$i^*((k+1)T_s) = 3i^*(kT_s) - 3i^*((k-1)T_s) + i^*((k-2)T_s). \tag{7}$$

Finally, the switching state corresponding to the selected optimal voltage vector at the next sampling instant is generated by the VSI. The one-step delay compensation algorithm requires the two-step future load current at the $(k+2)$th instant to compensate for the unavoidable calculation delay present in practical controllers, which can be obtained by shifting the load current dynamics in (5) one-step forward [9]

$$i((k+2)T_s) = v((k+1)T_s) + \frac{T_s}{L}\left[v^{k+1} - Ri((k+1)T_s) - e((k+1)T_s)\right]. \tag{8}$$

In addition, the two-step predicted current reference $i^*((k+2)T_s)$ can be also obtained by shifting the future current reference $< bold > i^* < /bold > (k+1)$ in (7) one-step forward

$$i^*((k+2)T_s) = 3i^*((k+1)T_s) - 3i^*(kT_s) + i^*((k-1)T_s). \tag{9}$$

The future back emf vector can be estimated by assuming that the future back emf vector is equal to the present back emf vector because the back emf vector varies at a much lower frequency compared with the fast sampling frequency. The present back emf vector can be calculated from (5) as

$$e((k+1)T_s) \approx \hat{e}(kT_s) = v^k - Ri(kT_s) - \frac{L}{T_s}\left[i((k+1)T_s) - i(kT_s)\right]. \tag{10}$$

The references and predicted load currents at $(k+2)$th steps are evaluated using the cost function in (6) with the currents at $(k+2)$th steps in the model predictive control method with the one-step delay compensation algorithm. Fig. 3 illustrates the block diagram of the conventional model predictive control method for the three-phase VSI with the one-step delay compensation algorithm. As clearly shown in Fig. 3, only one voltage vector selected among the seven possible voltage vectors including the zero vectors is applied during one entire sampling period. Thus, the conventional method utilizes the optimization process only to select the best voltage vector, whereas the selected vector is maintained for at least one sampling period.

III. Proposed RCMV-MPC Methods for VSIs

The common-mode voltage of the VSI shown in Fig. 1, defined as the potential between the load neutral point and the center of the dc-bus of the VSI, can be expressed with the pole voltages with respect to the midpoint of the dc-link voltage as [10]

$$v_{n0} = \frac{v_{a0} + v_{b0} + v_{c0}}{3}. \tag{11}$$

Since the VSI only takes the leg voltages on the discrete voltage levels with $\pm V_{\rm dc}/2$, the common-mode voltage of the VSI becomes $\pm V_{\rm dc}/6$ and $\pm V_{\rm dc}/2$ with the nonzero active vectors and the zero vectors applied to the VSI, respectively. Because the zero vectors lead to the highest common-mode voltages, the proposed RCMV-MPC methods I and II realize the model predictive control algorithm with only six nonzero active vectors to avoid utilizing the zero vectors. However, employing only the six nonzero vectors for the control of load current might lead to increased current ripples and increased current errors between the references and the actual load currents owing to the reduced number of usable voltage states. Taking into account that the zero vectors generally result in the smallest variations on load dynamics, increasing current ripples is unavoidable in controlling the load currents without the zero vectors. Therefore, the proposed methods utilize two nonzero voltage vectors in one sampling period to compensate for the reduced number of usable voltage vectors and achieve satisfactory performance of load current ripple and current errors even without using the zero vectors. During one sampling period T_s, two selected nonzero vectors are applied to the load at respective intervals, which are calculated to minimize the load current errors. In the proposed methods, one sampling period is divided into two intervals, which changes at every sampling period, as

$$T_1^k + T_2^k = T_s \tag{12}$$

where T_1^k and T_2^k are the time intervals when the first nonzero voltage vector v_1^k and the second nonzero vector v_2^k, respectively, are applied during the *k*th sampling period. Both the time intervals should be larger than zero and smaller than the sampling period T_s. Using (12), the current dynamics in (6) for the one-step future load current generated by the two nonzero vectors can be expressed as

$$i((k+1)T_s) = i(kT_s) + \frac{T_1^k}{L}\left[v_1^k - Ri(kT_s) - e(kT_s)\right] + \frac{T_2^k}{L}\left[v_2^k - Ri(kT_s + T_1^k) - e(kT_s + T_1^k)\right]. \tag{13}$$

Since the back emf vector changes at a much lower frequency compared with the fast sampling frequency, the two back emf vectors in one sampling period can be assumed to be equal as

$$e(kT_s) \approx e(kT_s + T_1^k). \tag{14}$$

Furthermore, similar to the calculation shown in (10), the present back emf vector of the proposed RCMV-MPC method required in (13) is calculated with the assumption of the vector being equal to the one-step past back emf by shifting (13) one-step backward as

$$\boldsymbol{e}(kT_s) \approx \hat{e}((k-1)T_s) = \frac{T_1^{k-1}}{T_s}\left[v_1^{k-1} - Ri((k-1)T_s)\right] + \frac{T_2^{k-1}}{T_s}\left[v_2^{k-1} - Ri((k-1)T_s + T_1^{k-1})\right] - \frac{L}{T_s}\left[i(kT_s) - i((k-1)T_s)\right]. \tag{15}$$

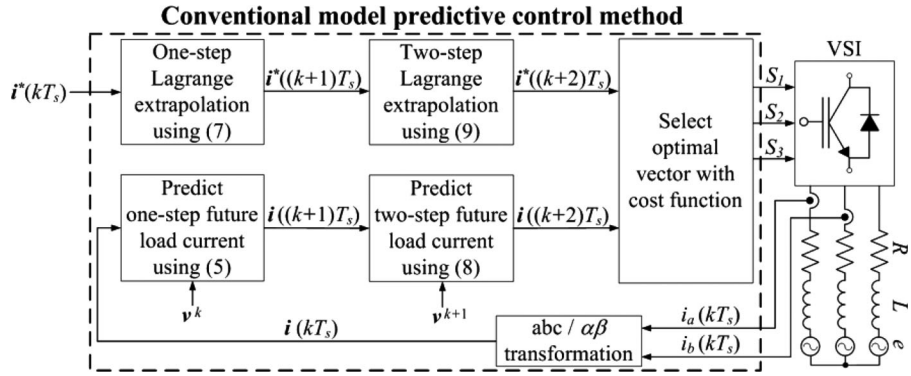

Fig. 3. Block diagram of the conventional model predictive control method.

In order to eliminate the adverse effects of the inevitable control delay of the proposed RCMV-MPC methods, the two-step prediction for the load current, as in (8), is required at the *k*th instant, as in the conventional model predictive control method. At the *k*th instant, the one-step future load current $i((k+1)T_s)$ required in (8) can be calculated from (13) by using the measured present load current $i(kT_s)$ as well as the two vectors v_1^k and v_2^k, and their corresponding time durations, T_1^k and T_2^k, respectively. On the basis of the calculated one-step future load current $i\left((k+1)T_s\right)$, the six possible nonzero voltage vectors at the $(k+1)$th instant lead to the six consequent predictions of the load current $i\left((k+2)T_s\right)$at the $(k+2)$th instant in (8). The future back emf vector required in (8) is, using (14), estimated by assuming that the future back emf vector be equal to the present back emf vector as

$$\begin{aligned} e\left((k+1)T_s\right) \approx \hat{e}(kT_s) &= \frac{T_1^k}{T_s}\left[v_1^k - Ri(kT_s)\right] \\ &+ \frac{T_2^k}{T_s}\left[v_2^k - Ri(kT_s + T_1^{k-1})\right] \\ &- \frac{L}{T_s}\left[i\left((k+1)T_s\right) - i(kT_s)\right]. \end{aligned} \quad (16)$$

On the basis of (8), (9), (13), (15), and (16), the two nonzero voltage vectors at the $(k+2)$th instant can be selected among the six nonzero voltage vectors from the cost function defined as

$$\begin{aligned} g = &\left\{i_\alpha^*\left((k+2)T_s\right) - i_\alpha\left((k+2)T_s\right)\right\}^2 \\ &+ \left\{i_\beta^*\left((k+2)T_s\right) - i_\beta\left((k+2)T_s\right)\right\}^2 \end{aligned} \quad (17)$$

where $i_\alpha\left((k+2)T_s\right)$ and $i_\beta\left((k+2)T_s\right)$ are the $\alpha\beta$ components of the load current at the $(k+2)$th instant, respectively. In addition, $i_\alpha^*\left((k+2)T_s\right)$ and $i_\beta^*\left((k+2)T_s\right)$ are the $\alpha\beta$ components of the reference current at the $(k+2)$th instant. The two-step predicted current reference $i^*\left((k+2)T_s\right)$ required in (17) can be obtained from (10). Thus, the two nonzero vectors, v_1^{k+1} and v_2^{k+1}, which result in the two smallest values from the cost function in (17), can be selected.

Once v_1^{k+1} and v_2^{k+1} are selected, the respective durations T_1^{k+1} and T_2^{k+1} for which they are applied in one sampling period should be determined. The two-step predicted load current $i\left((k+2)T_s\right)$ generated by the proposed RCMV-MPC method I can be calculated as

$$\begin{aligned} i\left((k+2)T_s\right) &= i\left((k+1)T_s\right) \\ &+ \frac{T_1^{k+1}}{L}\left[v_1^{k+1} - Ri\left((k+1)T_s\right) - e\left((k+1)T_s\right)\right] \\ &+ \frac{T_2^{k+1}}{L}\Big[v_2^{k+1} - Ri\left((k+1)T_s + T_1^{k+1}\right) \\ &- e\left((k+1)T_s + T_1^{k+1}\right)\Big]. \end{aligned} \quad (18)$$

The durations T_1^{k+1} and T_2^{k+1} are optimally distributed within one sampling period in such a way as to minimize the squared errors of the instantaneous $\alpha\beta$-axis components of the reference and actual currents based on the cost function. The optimal duration to distribute the two nonzero vectors is calculated from (17) as

$$\frac{\partial g}{\partial T_1^{k+1}} = 0. \quad (19)$$

Using (13), (16), (18), and (19), the future optimal duration T_1^{k+1} for the $(k+1)$th first nonzero vector v_1^{k+1} is determined as

$$T_1^{k+1} = \frac{V_{d\alpha}\left[Le_{2\alpha} + T_s(V_{d\alpha} - V_{L\alpha})\right] + V_{d\beta}\left[Le_{2\beta} + T_s(V_{d\beta} - V_{L\beta})\right]}{(V_{d\alpha})^2 + (V_{d\beta})^2} \quad (20)$$

where $V_{dm} = v_{1m}^{k+1} - v_{2m}^{k+1}$, $V_{Lm} = v_{1m}^{k+1} - Ri_m\left((k+1)T_s\right) - \hat{e}_m(kT_s)$, $e_{2m} = i_m^*\left((k+2)T_s\right) - i_m\left((k+1)T_s\right)$, and $m = \alpha, \beta$. The remaining duration T_2^{k+1} for the second nonzero vector v_2^{k+1} can be automatically determined from (12) and (20) as

$$T_2^{k+1} = T_s - T_1^{k+1}. \quad (21)$$

Note that the effect of the on-time of the first voltage vector on the changes in the current is neglected in calculating in (20) in the proposed method I, by assuming that the change in the load current vector operating at the fast sampling frequency is relatively small compared to the sudden

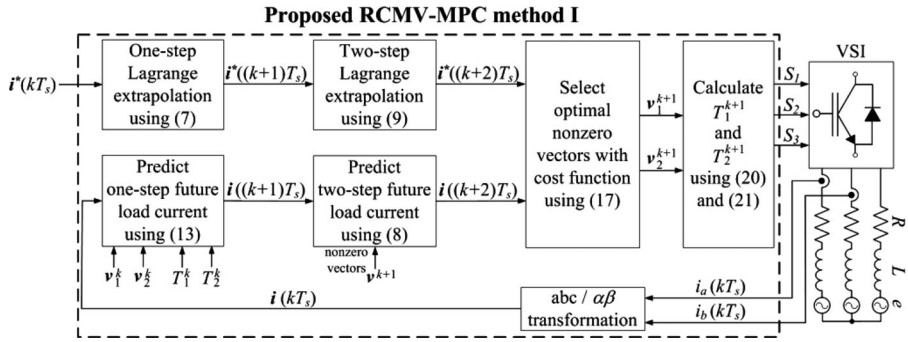

Fig. 4. Block diagram of the proposed RCMV-MPC method I.

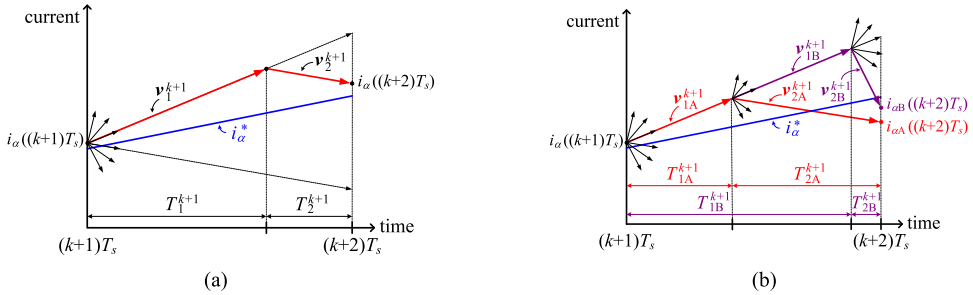

Fig. 5. Examples of α-axis current behaviors generated by (a) the proposed RCMV-MPC method I (b) the proposed RCMV-MPC method II.

change of the two voltage vectors applied in one sampling period as $i\left((k+1)T_s\right) \approx i\left((k+1)T_s + T_1^{k+1}\right)$. Considering the inevitable delay in the controller, the control processes for the proposed RCMV-MPC method I executed during the *k*th sampling period are applied in the following steps to compensate for the control delay:

1) measuring the load current $i(kT_s)$ at the kth instant;
2) applying the two nonzero VSI voltage vectors v_1^k and v_2^k during T_1^k and T_2^k, respectively, which were determined in the previous interval;
3) predicting the (k + 1)th load current $i\left((k+1)T_s\right)$ using (13);
4) predicting the six (k + 2)th load currents $i\left((k+2)T_s\right)$ obtained by the six possible nonzero active voltage vectors v^{k+1} using (8);
5) calculating the (k+2)th load current reference $i^*\left((k+2)T_s\right)$ using (9);
6) selecting the two nonzero vectors v_1^{k+1} and v_2^{k+1} on the basis of the cost function in (17);
7) determining the optimal durations T_1^{k+1} and T_2^{k+1} using (20) and (21); and
8) storingv_1^{k+1}, v_2^{k+1}, T_1^{k+1}, and T_2^{k+1} for application at the beginning of the next $(k+1)$th sampling instant.

By applying the delay compensation technique, almost one sampling period can be assigned for the calculations and predictions required to determine the two nonzero voltage vectors and the respective durations. Fig. 4 shows the overall block diagram of the proposed RCMV-MPC method I with the two nonzero voltage vectors.

In the proposed RCMV-MPC method I, application durations of the two selected nonzero vectors are determined to minimize the current errors, whereas the two nonzero vectors are simultaneously selected as the same as the conventional method. Therefore, in the proposed method I, the effects of the first vector and its on-time duration on selecting the second vector are neglected, for the purpose of implementing the algorithm without increasing the calculation complexity significantly. Contrary to the proposed RCMV-MPC method I, not only the selection of nonzero voltage vectors but also their application durations in the future sampling period are included in an optimization process in the proposed RCMV-MPC method II, to reduce current errors and ripples even without employing the zero vectors. Thus, an optimal set of two nonzero voltage vectors with variable application intervals, which are optimally determined at every sampling period, can lead to high-quality load current waveforms as well as reduced common-mode voltages, even with the reduced number of usable vectors. The proposed method II in advance selects the first nonzero voltage vector as same as the conventional method among the six nonzero vectors, on the basis of the cost function *g* in (17). Then, the six applicable nonzero voltage vectors from $\mathbf{V}_1$ to $\mathbf{V}_6$, including the preselected first nonzero voltage vector, are again considered as the second nonzero vectors. With respective second nonzero vector, the proposed method II calculates the application durations to apply the first and the second nonzero voltage vectors in such a way to result in the smallest current errors in the future sampling period. As a result, totally six sets consisting of two nonzero voltage vectors and the corresponding application intervals of the two nonzero vectors are evaluated in the proposed method II, whereas the proposed method I judges only one set with the two nonzero vectors. This is because the proposed method II selects the second nonzero vector by considering the effects of the first nonzero vector and

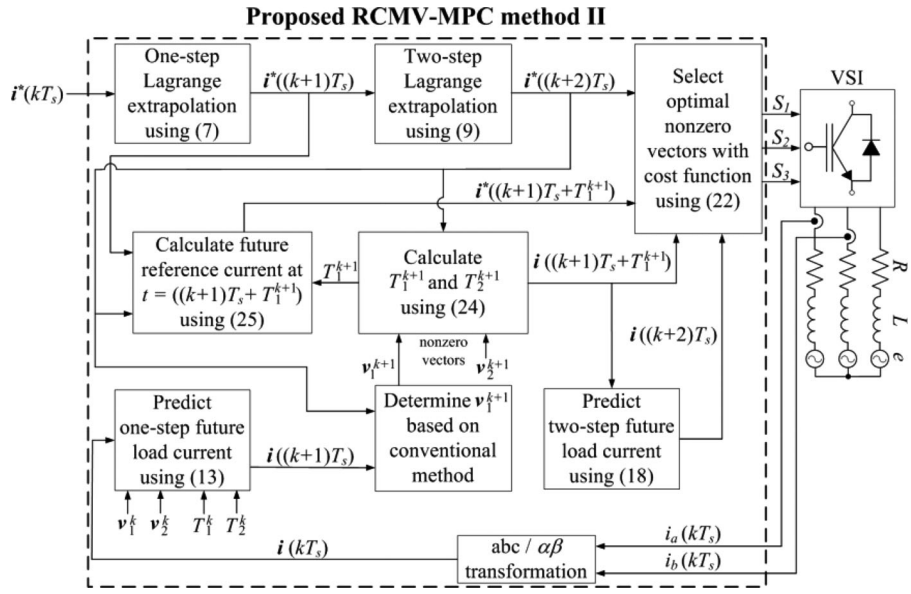

Fig. 6. Block diagram of the proposed RCMV-MPC method II.

its on-time duration, contrary to the proposed method I. Fig. 5 shows the difference of the operation principles to select the second vector in the proposed methods I and II. Among six possible nonzero voltage vector sets obtained by the proposed method II, one optimal set with two nonzero vectors used in the future sampling period is selected to force the actual load current to track the reference during the next sampling instant as close as possible. In addition, the proposed algorithm II evaluates the six sets of the nonzero voltage vectors on the basis of two evaluating instants, for the purpose of selecting an optimal set to generate load current trajectories with low current errors and current ripples. If the optimal set is selected on the basis of the evaluation only at the future sampling instant, a set to produce a large current error inside the future sampling period might be selected as an optimal one. Therefore, the proposed algorithm II evaluates the actual and the reference currents at next sampling instant as well as at a turning point of the two voltage vectors inside the future sampling period. Fig. 5(b) illustrates an example of the α-axis current trajectories generated by two nonzero voltage vectors in the proposed RCMV-MPC method II. Although the set with v_{1B}^{k+1} and v_{2B}^{k+1} results in the smaller current error at the end of the sampling instant, the current behavior generated by the set with v_{1A}^{k+1} and v_{2A}^{k+1} leads to better tracking capability during the whole sampling period. Thus, the proposed method II selects the optimal set with the two nonzero vectors on the basis of the cost function defined at two evaluating instants, which are a turning point of the two nonzero vectors as well as at the next sampling instant. It should be noted that the turning point of the two nonzero vectors varies depending on the each second nonzero vector. Therefore, the proposed method II evaluates the six voltage sets on the basis of the two instants, which of one is varying and the other one is fixed. The optimal set with the smallest cost function calculated at the two evaluation instants in the future sampling period is selected and is applied at the next sampling period in the proposed method II.

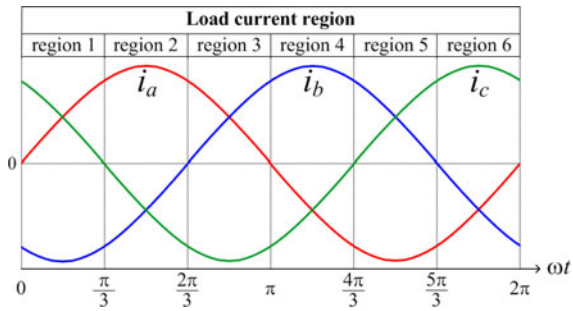

Fig. 7. Effective voltage vectors generated when all the six IGBTs are OFF.

For the purpose of selecting the optimal nonzero vector set in terms of the current errors, the proposed RCMV-MPC method II utilizes the cost function defined at two instants as

$$\begin{aligned} G &= \left\{i_\alpha^*\left((k+2)T_s\right) - i_\alpha\left((k+2)T_s\right)\right\}^2 \\ &+ \left\{i_\beta^*\left((k+2)T_s\right) - i_\beta\left((k+2)T_s\right)\right\}^2 \\ &+ \left\{i_\alpha^*\left((k+1)T_s + T_1^{k+1}\right) - i_\alpha\left((k+1)T_s + T_1^{k+1}\right)\right\}^2 \\ &+ \left\{i_\beta^*\left((k+1)T_s + T_1^{k+1}\right) - i_\beta\left((k+1)T_s + T_1^{k+1}\right)\right\}^2. \end{aligned} \tag{22}$$

Once the first nonzero vector is preselected by the cost function g in the conventional algorithm, the durations of the two nonzero vectors applied in the future sampling period, T_1^{k+1} and T_2^{k+1}, are determined by solving an optimization problem depending on the respective second nonzero vector. The durations, T_1^{k+1} and T_2^{k+1}, are optimally distributed within the future sampling period in such a way as to minimize the squared errors of the instantaneous $\alpha\beta$-axis components of the reference and actual currents with respect to the durations. The optimal

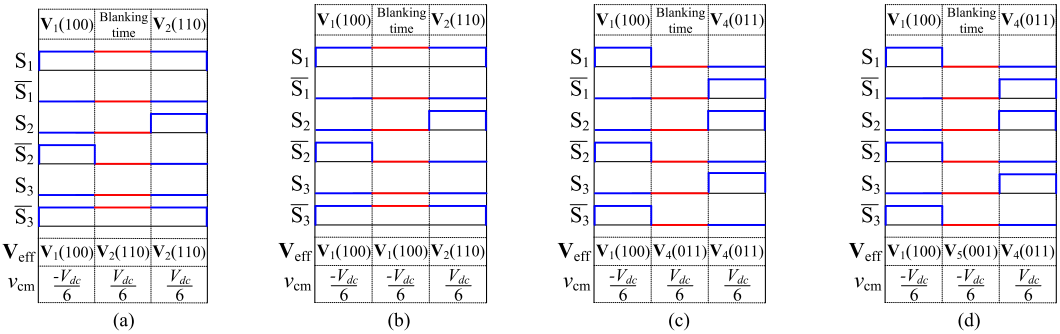

Fig. 8. Examples of switching patterns and common-mode voltage during the blanking time in case of the transitions in (a) one VSI leg at region 2, (b) one VSI leg at region 3, (c) three VSI legs at region 2, and (d) three VSI legs at region 3.

TABLE I
EFFECTIVE VOLTAGE VECTORS GENERATED DURING THE BLANKING TIME WHEN THE SWITCHING TRANSITIONS OCCUR IN THREE VSI LEGS

Load current region	region 1	region 2	region 3	region 4	region 5	region 6
Effective voltage vector	$\mathbf{V}_3$	$\mathbf{V}_4$	$\mathbf{V}_5$	$\mathbf{V}_6$	$\mathbf{V}_1$	$\mathbf{V}_2$

duration to distribute the two nonzero vectors is calculated as

$$\frac{\partial G}{\partial T_1^{k+1}} = 0. \tag{23}$$

By reflecting (9), (13), (18), and (22) into (23), the future optimal duration for the first future nonzero vector is determined as (24) shown at the bottom of the page where $e_{1m} = i_m^* ((k+1)T_s) - i_m ((k+1)T_s)$, $i_{dm}^* = i_m^* ((k+2)T_s) - i_m^* ((k+1)T_s)$, and $m = \alpha, \beta$. The remaining duration of the second nonzero vector, T_2^{k+1}, is then decided using (12) and (24). In order to compare the actual load current and the reference current at the turning point $t = (k+1)T_s + T_1^{k+1}$, the reference current at the instant $t = (k+1)T_s + T_1^{k+1}$ is required as well. Thus, the reference current value at the turning point $t = (k+1)T_s + T_1^{k+1}$ at the future step is calculated as

$$i^* \left((k+1)T_s + T_1^{k+1}\right) = i^* ((k+1)T_s) + \frac{T_1^{k+1}}{T_s} \left\{i^* ((k+2)T_s) - i^* ((k+1)T_s)\right\} \tag{25}$$

Thus, the reference current value $i^* \left((k+1)T_s + T_1^{k+1}\right)$ can be obtained for the respective second nonzero vector once the application time of the first nonzero voltage vector T_1^{k+1} is calculated in (24). Based on the cost function in (22), the optimal future set with the two nonzero vectors and their optimal durations to generate the smallest current errors inside the future sampling period as well as at the future sampling instant can be selected, among the six candidates. As a result, the two future nonzero voltage vectors determined in the proposed algorithm II are applied during the predetermined duration in the future sampling period. Fig. 6 shows the block diagram of the

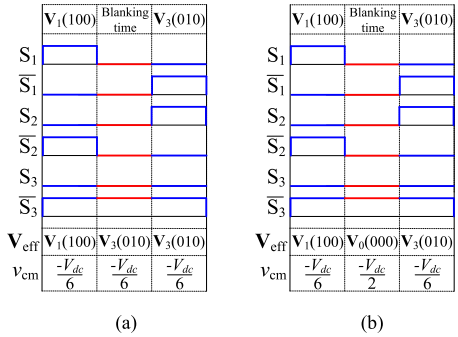

Fig. 9. Examples of switching patterns and common-mode voltage in case of the simultaneous transitions in two VSI legs (a) at region 2 and (b) at region 3.

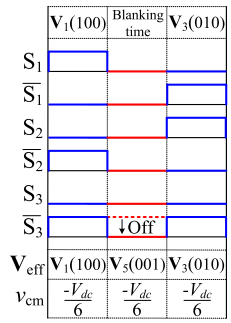

Fig. 10. Switching patterns to reduce the common-mode voltage during the blanking time in case of the simultaneous transitions in two VSI legs at region 3.

$$T_1^{k+1} = \frac{V_{d\alpha}\left[Le_{2\alpha} + T_s(V_{d\alpha} - V_{L\alpha})\right] + V_{d\beta}\left[Le_{2\beta} + T_s(V_{d\beta} - V_{L\beta})\right] - L\left\{e_{1\alpha}\left(\frac{L}{T_s}i_{d\alpha}^* - V_{L\alpha}\right) + e_{1\beta}\left(\frac{L}{T_s}i_{d\beta}^* - V_{L\beta}\right)\right\}}{(V_{d\alpha})^2 + (V_{d\beta})^2 + \left(\frac{L}{T_s}i_{d\alpha}^* - V_{L\alpha}\right)^2 + \left(\frac{L}{T_s}i_{d\beta}^* - V_{L\beta}\right)^2} \tag{24}$$

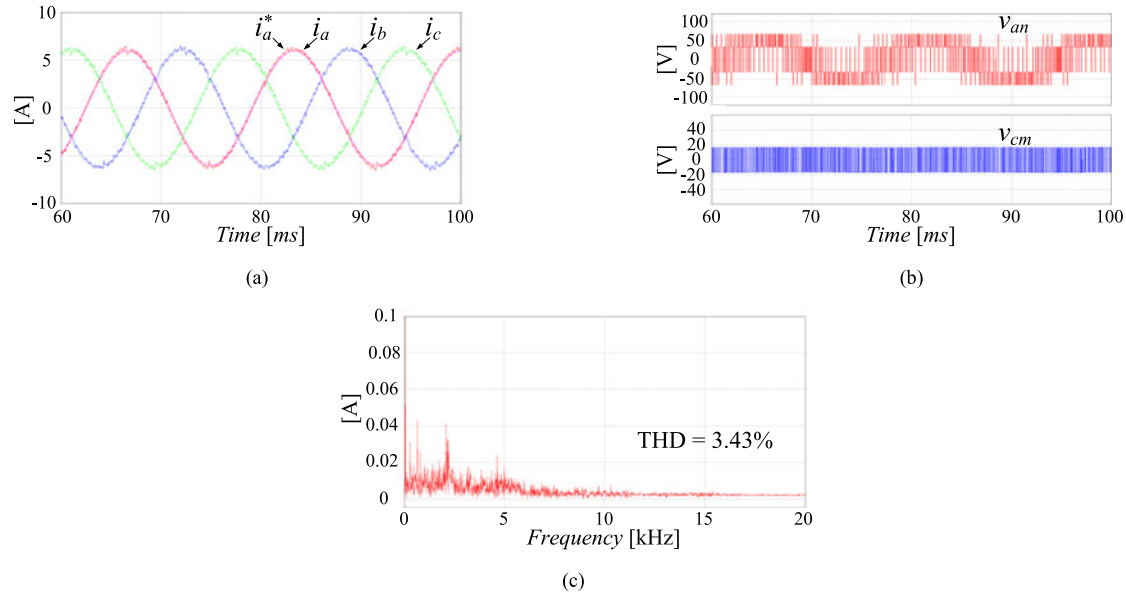

Fig. 11. Simulated waveforms of the proposed RCMV-MPC method I with $T_s = 100\ \mu$s: (a) the three-phase load currents (i_a, i_b, and i_c) and a-phase reference current (i_a^*), (b) phase voltage (v_{an}) and common-mode voltage ($v_{\rm cm}$), and (c) frequency spectrum of the a-phase load current ($I^* = 6$ A and $V_{\rm dc} = 100$ V).

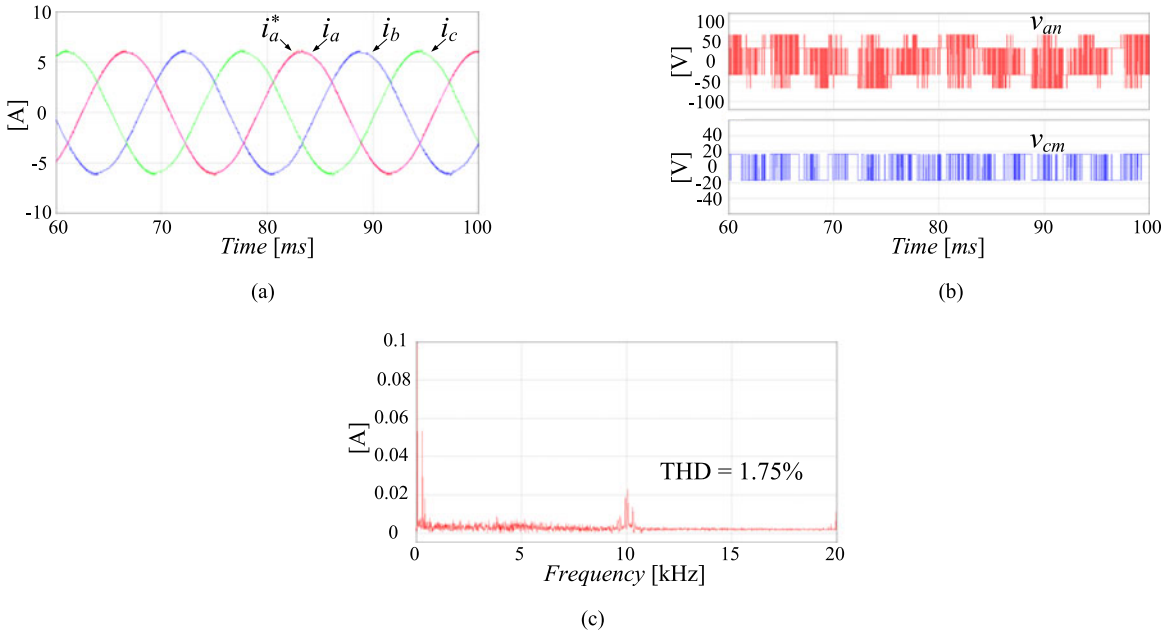

Fig. 12. Simulated waveforms of the proposed RCMV-MPC method II with $T_s = 100\ \mu$s: (a) the three-phase load currents (i_a, i_b, and i_c) and a-phase reference current (i_a^*), (b) phase voltage ($v_{\rm an}$) and common-mode voltage ($v_{\rm cm}$), and (c) frequency spectrum of the a-phase load current ($I^* = 6$ A and $V_{\rm dc} = 100$ V).

proposed method II. The block diagrams in Figs. 3, 4, and 6 clearly show that the proposed RCMV-MPC methods I and II can be implemented with no additional measurements compared with the conventional method.

The common-mode voltage is sensitive to the blanking time of the IGBTs, where an effective voltage vector is generated by the uncontrollable load current conduction through the freewheeling diode during the blanking time. Because the model predictive control methods including the proposed methods select an optimal voltage vector at every sampling period, switching transition is not limited to adjacent vectors. Therefore, unlike the well-known space vector pulse width modulation method where only one leg is involved in every switching transition, the model predictive control methods can lead to the switching transitions in one, two, or three legs depending on the selected optimal voltage vector at the next step. Because the uncontrollable load current flows through the freewheeling diode during the blanking time, an effective voltage vector during the blanking time depends on the directions of the three-phase load currents. One fundamental period of the load currents can be classified into six

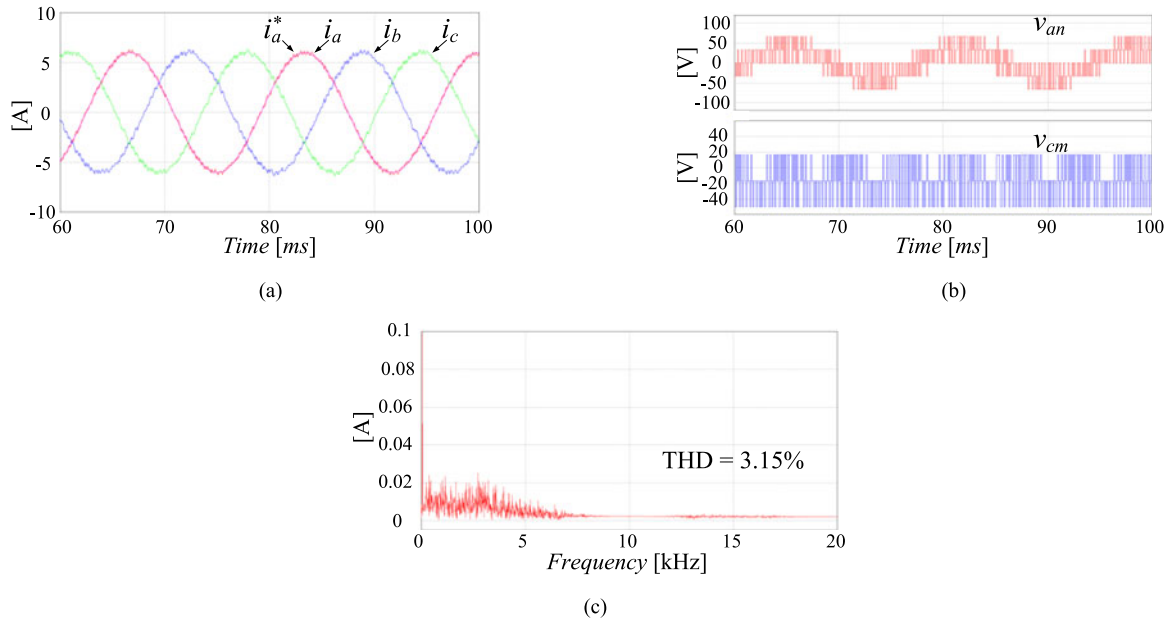

Fig. 13. Simulated waveforms of the conventional method with $T_s = 100$ μs: (a) the three-phase load currents (i_a, i_b, and i_c) and a-phase reference current (i_a^*), (b) phase voltage (v_{an}) and common-mode voltage ($v_{\rm cm}$), and (c) frequency spectrum of the a-phase load current ($I^* = 6$ A and $V_{\rm dc} = 100$ V).

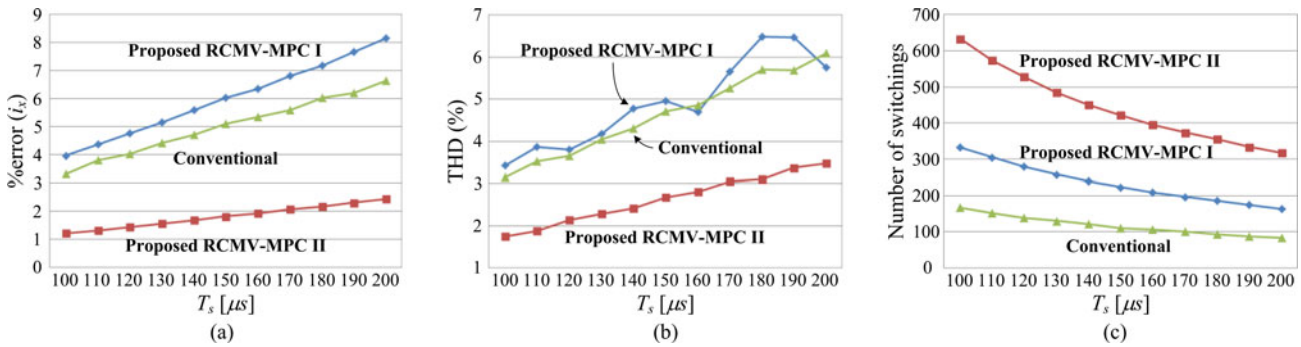

Fig. 14. Comparative results of the proposed RCMV-MPC methods I and II with the conventional method as a function of the sampling periods: (a) current errors of the load currents, (b) THD of the load currents, and (c) number of switchings ($V_{\rm dc} = 100$ V and $I^* = 6$ A).

regions in which none of the load currents change their polarities, as shown in Fig. 7. Thus, an effective voltage vector during the blanking time is determined according to which region the switching operation occurs at.

In the case that only one leg is involved in the switching operation, one of the six active vectors dependent on the load current directions is produced during the blanking time. In addition, all the six IGBTs in the VSI are open during the blanking time, when the switching transition simultaneously happens in all the three legs. Therefore, one of the six active vectors is generated as an effective voltage vector during the blanking time. Fig. 8 illustrates examples of the switching patterns and the common-mode voltages during the blanking time in the case of the transitions in one and three VSI legs, respectively. In particular, in the case of the switching transitions in three VSI legs, an effective voltage vector during the blanking time is entirely determined by the region, where the switching transition happens, because all the three IGBTs are OFF during the blanking time. Table I shows the effective voltage vectors generated during the blanking time when the switching transitions occur in three VSI legs. Thus, it can be concluded that the blanking time involved in the transitions in one leg or three legs gives no adverse effects on reducing the common-mode voltage because the zero vectors are not generated during the blanking time.

However, simultaneous transitions in the two VSI legs might result in unplanned zero vectors during the blanking time, dependent on the direction of the load currents. Fig. 9 shows an example of the simultaneous switching transitions in two VSI legs at region 2 and at region 3, respectively. Whereas the effective voltage vector during the blanking time becomes the nonzero vector $\mathbf{V}_3$ at region 2, the zero vector $\mathbf{V}_0$ is generated during the blanking time at region 3. Therefore, simultaneous transitions in the two VSI legs result in the spontaneous zero vector and the increased common-mode voltage, which should be prevented to maintain the reduced common-mode voltage. In the case of simultaneous transitions in two VSI legs, the method to drive the

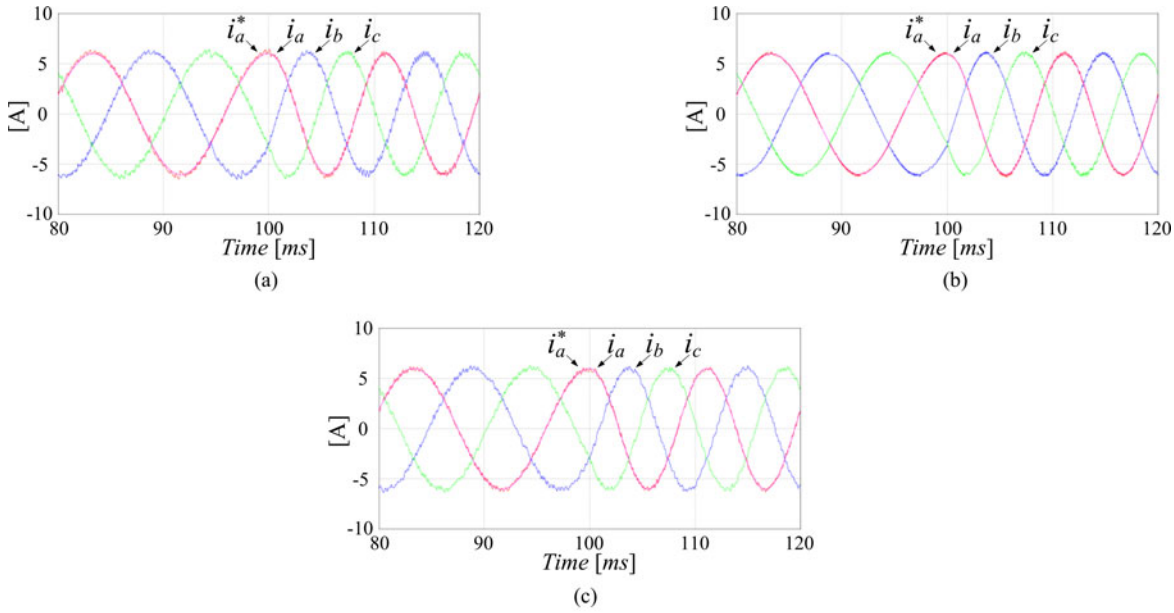

Fig. 15. Three-phase output currents (i_a, i_b, and i_c) and a-phase reference current (i_a^*) for a frequency step change from 60 to 90 Hz obtained from (a) the proposed RCMV-MPC method I for $T_s = 100$ μs, (b) the proposed RCMV-MPC method II for $T_s = 100$ μs, and (c) the conventional method for $T_s = 100$ μs.

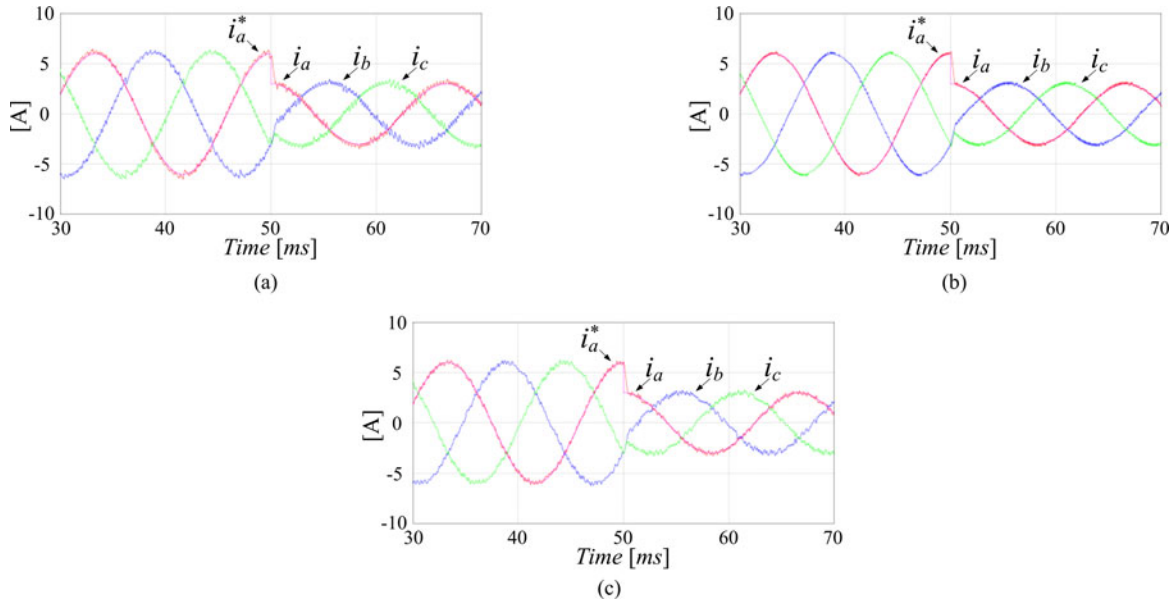

Fig. 16. Three-phase output currents (i_a, i_b, and i_c) and a-phase reference current ($i_a{}^*$) for a magnitude step change obtained from (a) the proposed RCMV-MPC method I for $T_s = 100$ μs, (b) the proposed RCMV-MPC method II for $T_s = 100$ μs, and (c) the conventional method for $T_s = 100$ μs.

three-phase load currents to flow only through the freewheeling diodes during the blanking time is, which is similar with the case of simultaneous switching of the three VSI legs, employed in the proposed RCMV-MPC methods to prevent the undesirable zero vectors from being produced during the blanking time [27]. As a result, during the blanking time in simultaneous transitions in the two VSI legs, all the IGBT are forced to OFF and the effective vector is restricted to the nonzero vectors, as shown in Fig. 10.

IV. Simulation Results

Figs. 11 and 12 show the simulated waveforms obtained from the proposed RCMV-MPC methods using only the nonzero voltage vectors with $V_{\rm dc} = 100$ V, $T_s = 100$ μs, and an RLe load with $R = 2.5$ Ω, $L = 10$ mH, and $e = 20$ V. For comparison, the simulated results of the conventional method with the zero vector $\mathbf{V}_0$ are shown in Fig. 13. The per-unit values for the voltage, current, impedance are 0.134 V, 0.142 A, 0.314 Ω, respectively, by assuming that the base voltage and base power

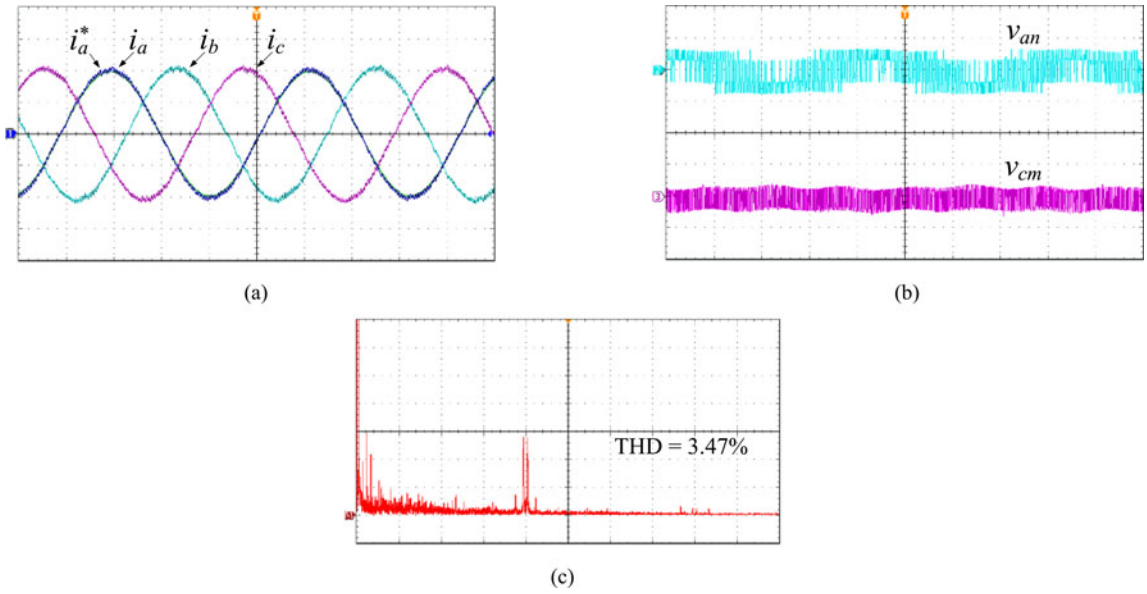

Fig. 17. Experimental waveforms of the RCMV-MPC method I with $T_s = 100$ μs: (a) the three-phase load currents (i_a, i_b, and i_c) and a-phase reference current (i_a^*) (3 A/div and 4 ms/div), (b) phase voltage (v_{an}) (100 V/div and 4 ms/div) and common-mode voltage ($v_{\rm cm}$) (50 V/div and 4 ms/div), and (c) frequency spectrum of the a-phase load current (10 mA/div and 1.25 kHz/div) ($I^* = 6$ A and $V_{\rm dc} = 100$ V).

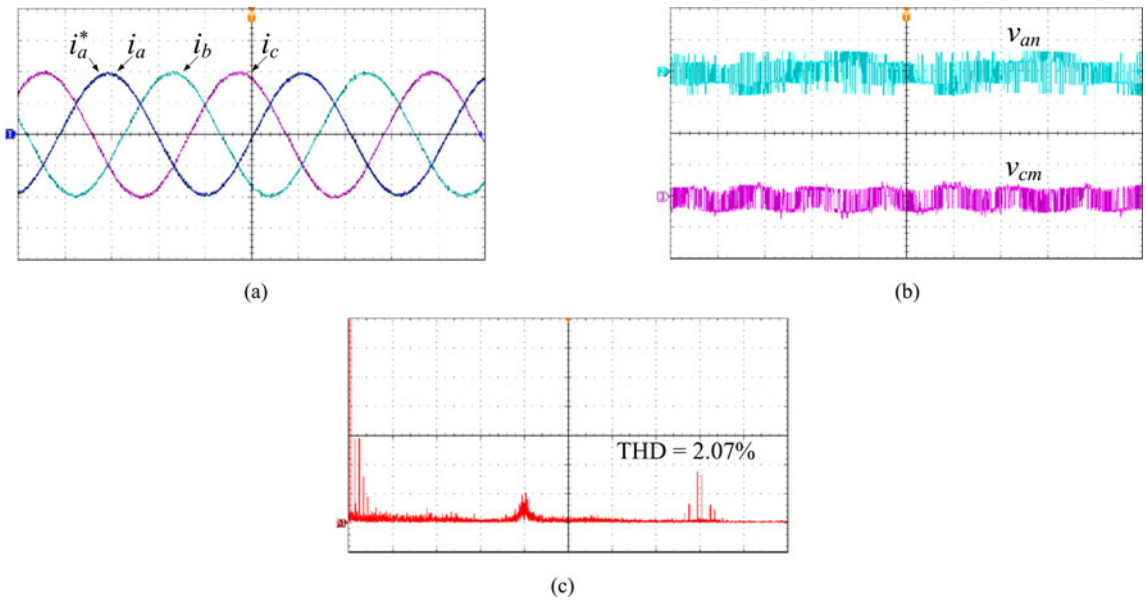

Fig. 18. Experimental waveforms of the RCMV-MPC method II with $T_s = 100$ μs: (a) the three-phase load currents (i_a, i_b, and i_c) and a-phase reference current (i_a^*) (3 A/div and 4 ms/div), (b) phase voltage (v_{an}) (100 V/div and 4 ms/div) and common-mode voltage ($v_{\rm cm}$) (50 V/div and 4 ms/div), and (c) frequency spectrum of the a-phase load current (10 mA/div and 1.25 kHz/div) ($I^* = 6$ A and $V_{\rm dc} = 100$ V).

are 750 V and 39 000 W, respectively. Figs. 11 and 12 show that the load currents generated by the two proposed RCMV-MPC methods accurately track their references. In addition, it is observed that the common-mode voltages of the proposed methods are limited to $\pm V_{\rm dc}/6$, whereas the conventional method generates a common-mode voltage oscillating between $V_{\rm dc}/6$ and $-V_{\rm dc}/2$ owing to the utilization of $\mathbf{V}_0$. The THD of the load current observed in the proposed RCMV-MPC method I is slightly higher than that in the conventional method, whereas the proposed RCMV-MPC II leads to lower THD value than the conventional method due to more sophisticated optimization algorithm. Because the proposed RCMV-MPC methods utilizes the two nonzero voltage vectors with their optimum duration, the proposed methods result in satisfactory waveform quality in comparison with the conventional method, despite the utilization of only six nonzero vectors.

The performance of the VSIs based on predictive control methods is strongly influenced by the sampling period because of the inherent operating principle. As a result, the performance of the VSI based on the two proposed RCMV-MPC methods

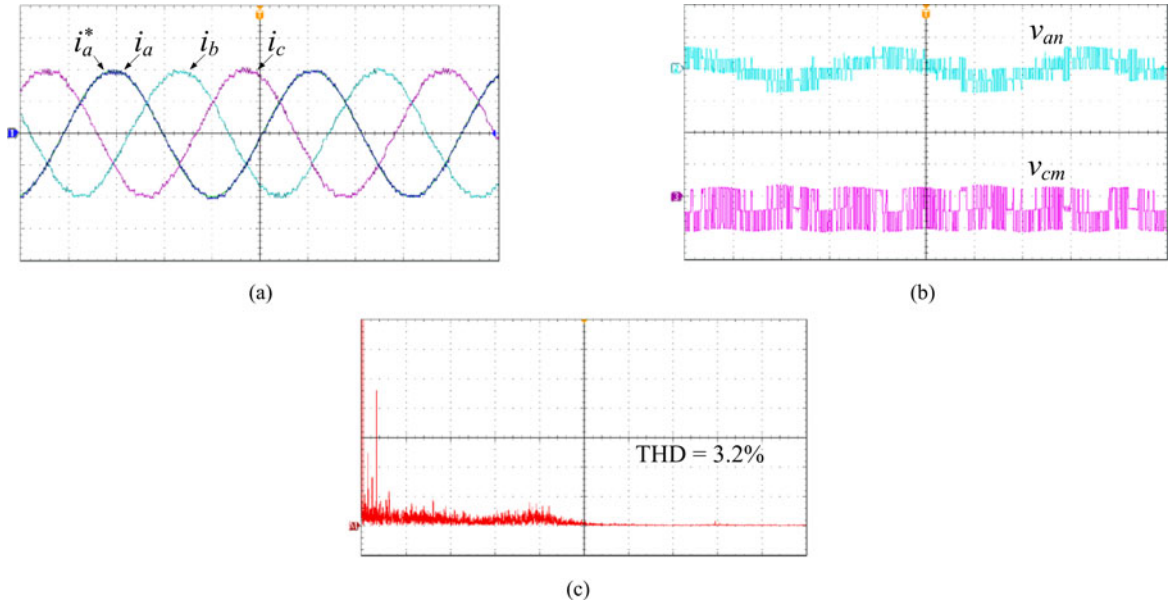

Fig. 19. Experimental waveforms of the conventional method with $T_s = 100\ \mu$s: (a) the three-phase load currents (i_a, i_b, and i_c) and a-phase reference current (i_a^*) (3 A/div and 4 ms/div), (b) phase voltage (v_{an}) (100 V/div and 4 ms/div) and common-mode voltage ($v_{\rm cm}$) (50 V/div and 4 ms/div), and (c) frequency spectrum of the a-phase load current (10 mA/div and 1.25 kHz/div) ($I^* = 6$ A and $V_{\rm dc} = 100$ V).

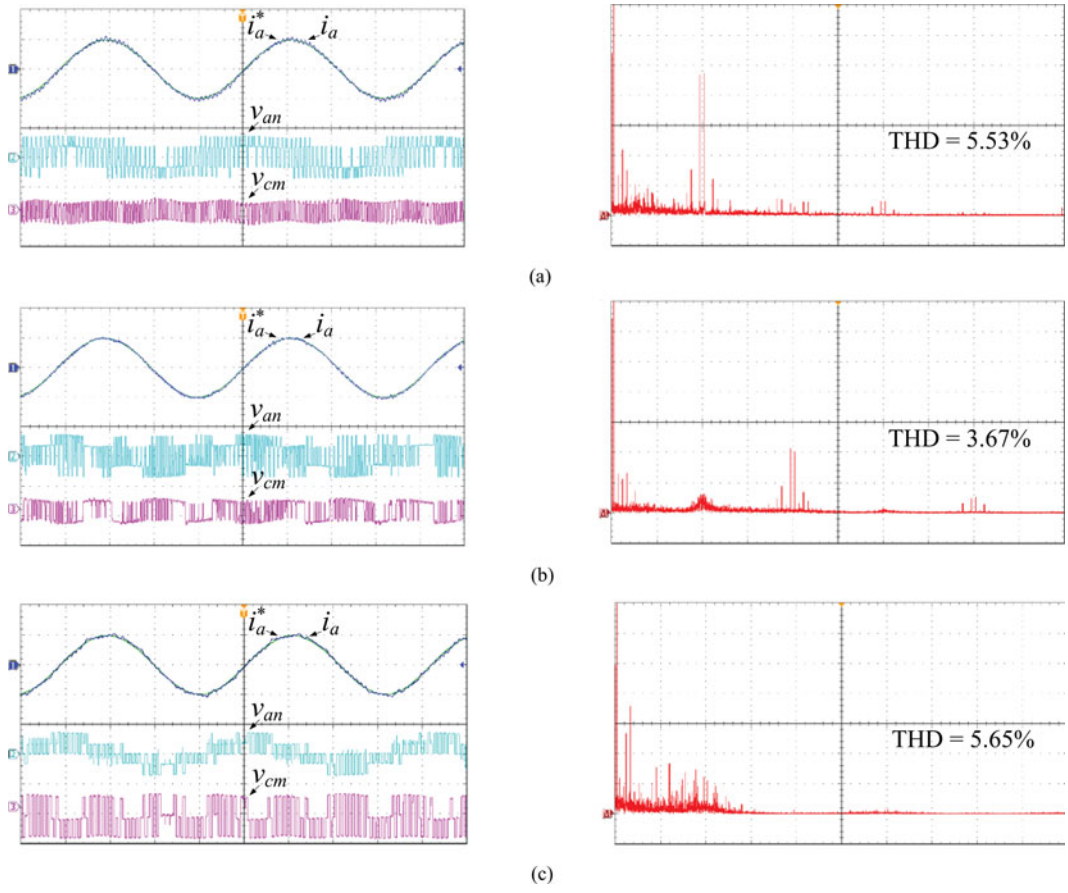

Fig. 20. Experimental waveforms with $T_s = 200\ \mu$s, the a-phase load current (i_a), a-phase reference current (i_a^*) (3 A/div and 4 ms/div), phase voltage (v_{an}) (100 V/div and 4 ms/div), common-mode voltage ($v_{\rm cm}$) (50 V/div and 4 ms/div), and frequency spectrum of the a-phase load current (20 mA/div and 1.25 kHz/div) obtained from (a) the proposed RCMV-MPC method I, (b) the proposed RCMV-MPC method II, and (c) the conventional method ($I^* = 6$ A and $V_{\rm dc} = 100$ V).

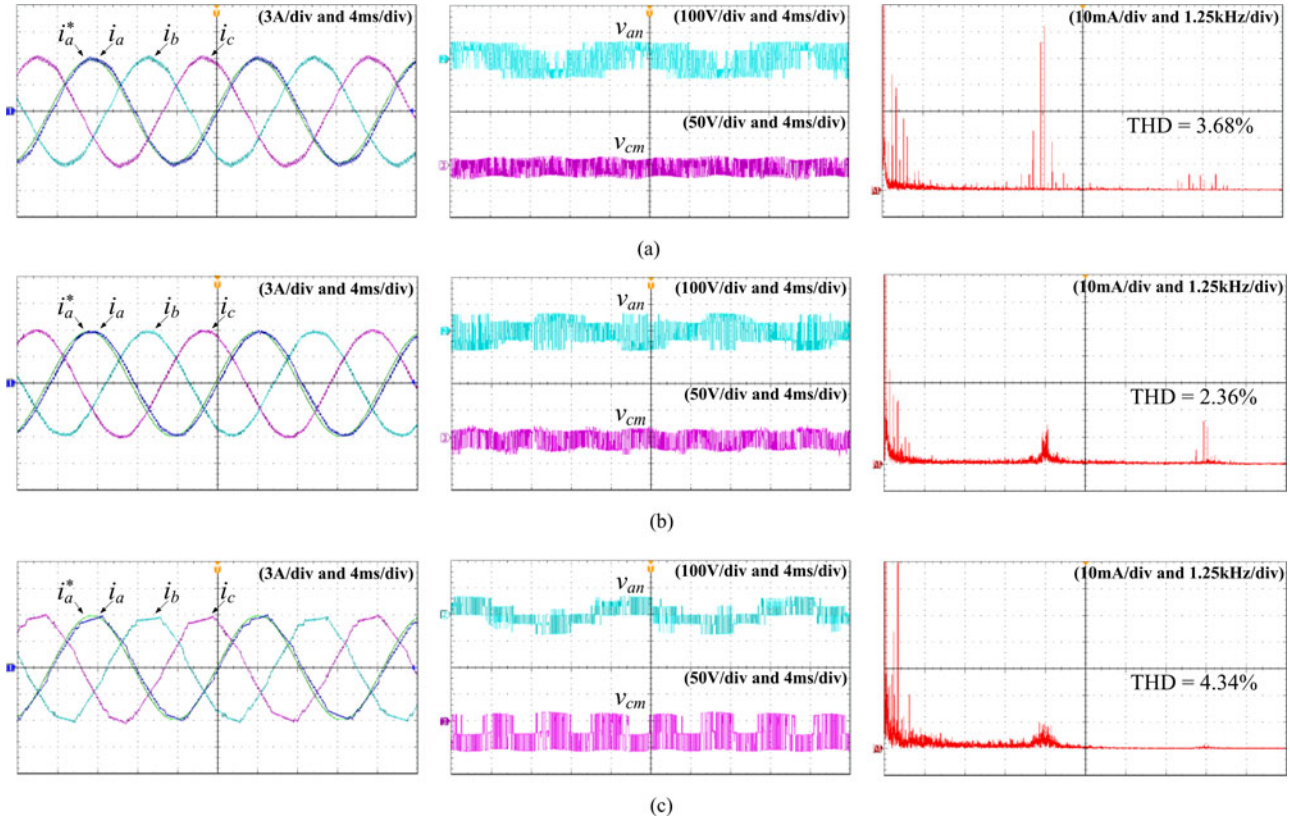

Fig. 21. Experimental waveforms with the 50% underestimated inductance and the exact resistance ($I^* = 6$ A, $T_s = 100$ μs, and $V_{\rm dc} = 100$ V) for (a) the proposed RCMV-MPC method I (b) the proposed RCMV-MPC method II, and (c) the conventional method.

are compared with that of the VSI based on the conventional model predictive control method in terms of current errors, THD of the load currents, and average number of switching transitions as a function of the sampling period, as shown in Fig. 14. Fig. 14(a) shows the percentages of the current errors obtained by the proposed RCMV-MPC I, II, and conventional methods versus the sampling period. The percentage of the current error is defined as the absolute difference between the reference and load currents normalized to the respective rms value of the load current references as

$$\%\text{error}(i_x) = \frac{\sum\limits_{x=a,b,c} \frac{1}{N} \sum\limits_{k=1}^{N} |i_x^*(k) - i_x(k)|}{\sum\limits_{x=a,b,c} \text{rms}(i_x^*(k))} \times 100 \qquad (26)$$

where the value of N is 20 000 per fundamental period of the output. The proposed RCMV-MPC method I yields slightly higher current errors than the conventional method because no zero vector utilization in the proposed RCMV-MPC method I decreases the current-tracking capability. On the other hand, the proposed RCMV-MPC method II leads to significantly lower current errors than the conventional method. Fig. 14(b) shows the THD percentages obtained by the proposed and conventional methods as a function of the sampling period. The THD percentage is defined as

$$\%\text{THD} = \frac{\sum\limits_{x=a,b,c} \sqrt{i_{x2}^2 + i_{x3}^2 + \cdots + i_{xn}^2}}{\sum\limits_{x=a,b,c} i_{x1}} \times 100 \qquad (27)$$

where i_{x1} and i_{xn} are the fundamental and nth-harmonic components of the load current in phase x, respectively. The number n was set to 8335 in the simulation. Fig. 14(b) shows that the proposed method I exhibits a slightly higher THD than the conventional method because of its operating principle with only nonzero vectors to reduce the common-mode voltage, whereas the proposed method II results in significantly lower THD values than the conventional method. Furthermore, the average numbers of the switching transitions, which are calculated by measuring the number of switching operations of the switches for 15 output periods, are shown in Fig. 14(c). It is seen that the two proposed methods increase the number of switching transitions in comparison with the conventional method because the proposed schemes employ two nonzero vectors during one sampling period to compensate for the reduced number of voltage vectors by avoiding the zero vectors. In addition, it is seen that the proposed RCMV-MPC II yields better performance in the current errors and the THD values at the expense of the increased number of switching transitions, in comparison with the proposed method I and the conventional method.

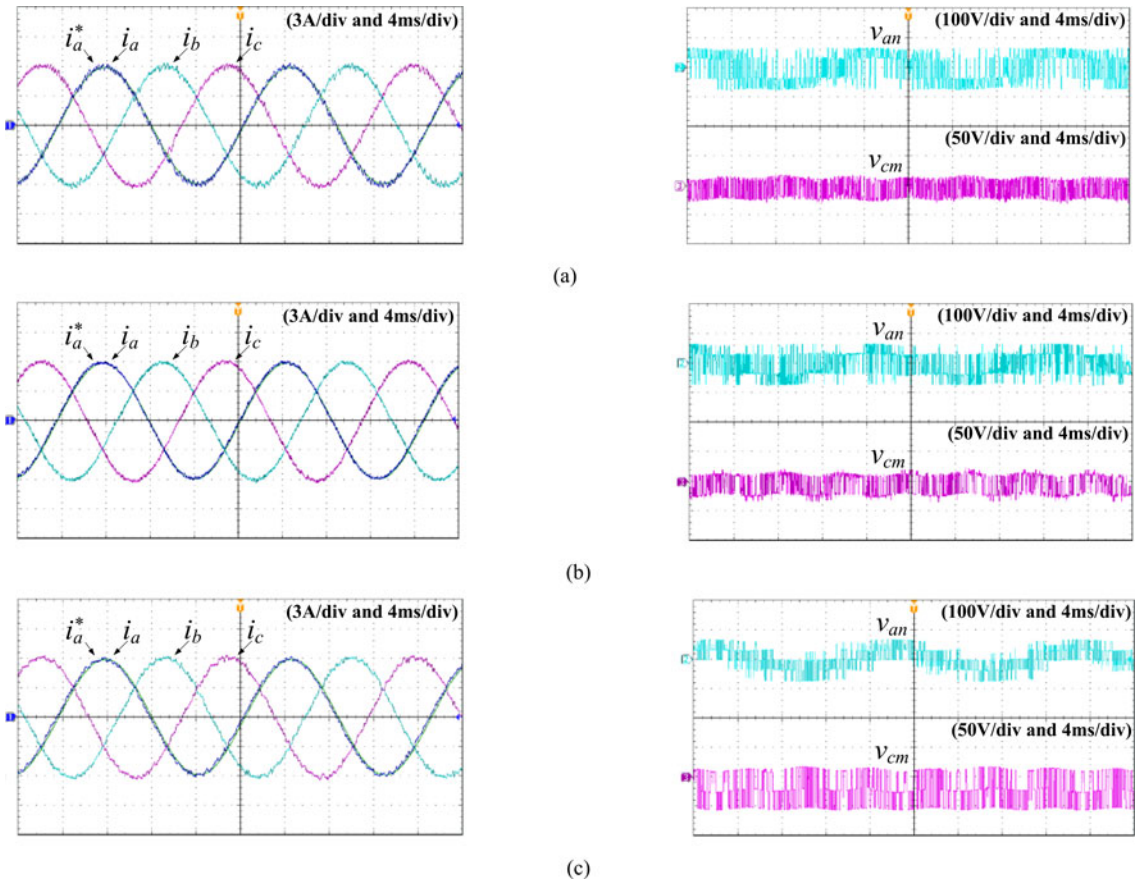

Fig. 22. Experimental waveforms with the 50% overestimated inductance and the correct resistance ($I^* = 6$ A, $T_s = 100$ μs, and $V_{\rm dc} = 100$ V) for (a) the proposed RCMV-MPC method I (b) the proposed RCMV-MPC method II, and (c) the conventional method.

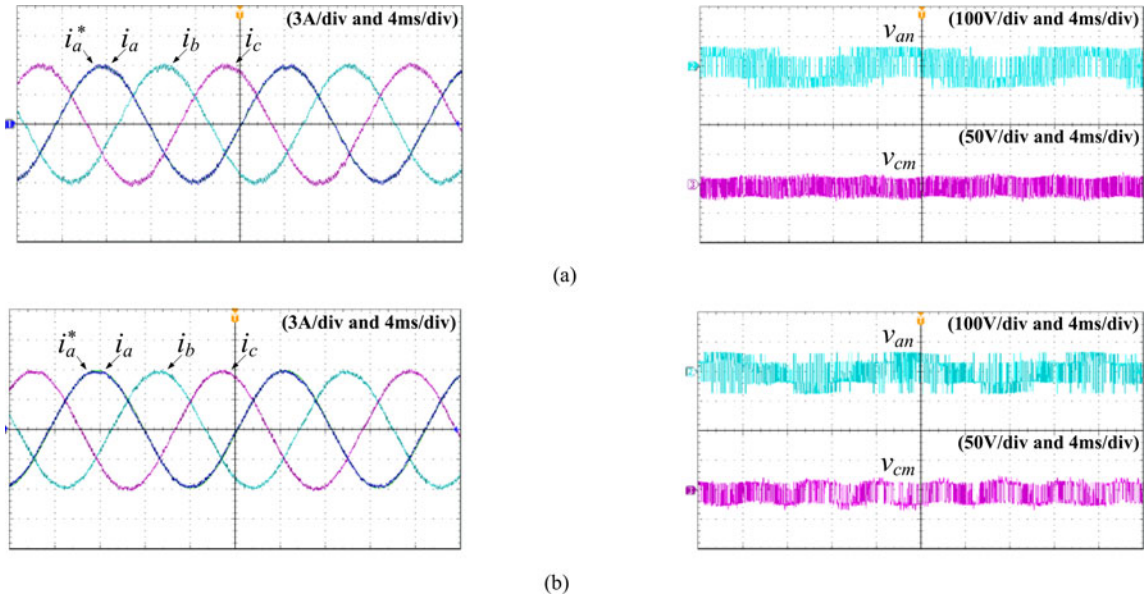

Fig. 23. Experimental waveforms with the correct inductance and 50% underestimated resistance ($I^* = 6$ A, $T_s = 100$ μs, and $V_{\rm dc} = 100$ V) for (a) the proposed RCMV-MPC method I and (b) the proposed RCMV-MPC method II.

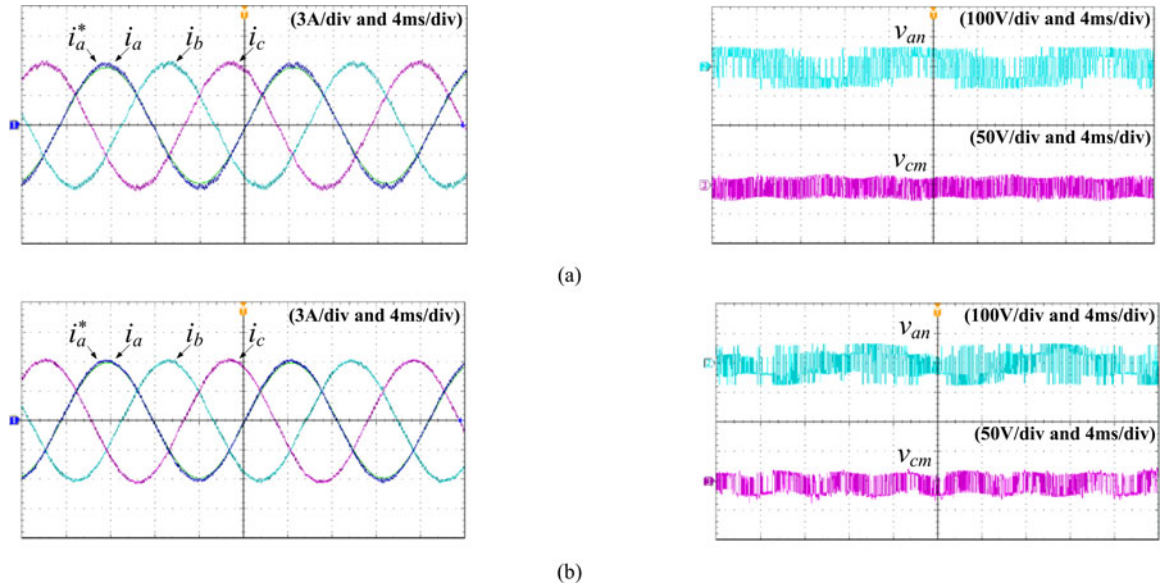

Fig. 24. Experimental waveforms with the correct inductance and 50% overestimated resistance ($I^* = 6$ A, $T_s = 100$ μs, and $V_{\rm dc} = 100$ V) for (a) the proposed RCMV-MPC method I and (b) the proposed RCMV-MPC method II.

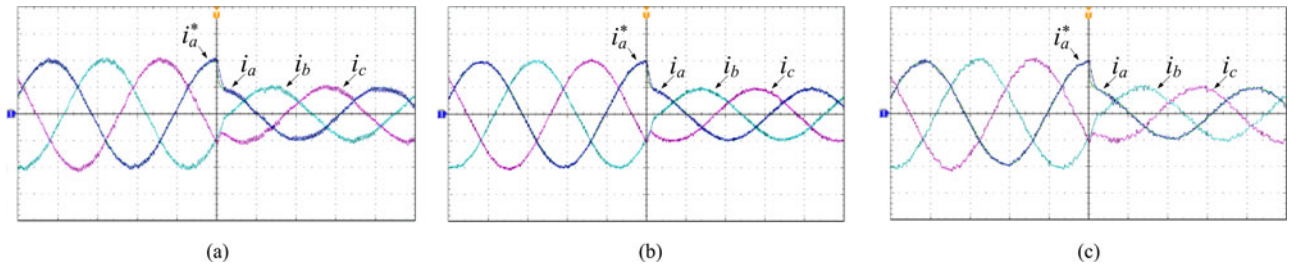

Fig. 25. Experimental waveforms of the three-phase load currents (i_a, i_b, and i_c) and a-phase reference current (i_a^*) (3 A/div and 4 ms/div) for a magnitude step change from 6 to 3 A for (a) the proposed RCMV-MPC method I, (b) the proposed RCMV-MPC method II, and (c) the conventional method ($T_s = 100$ μs and $V_{\rm dc} = 100$ V).

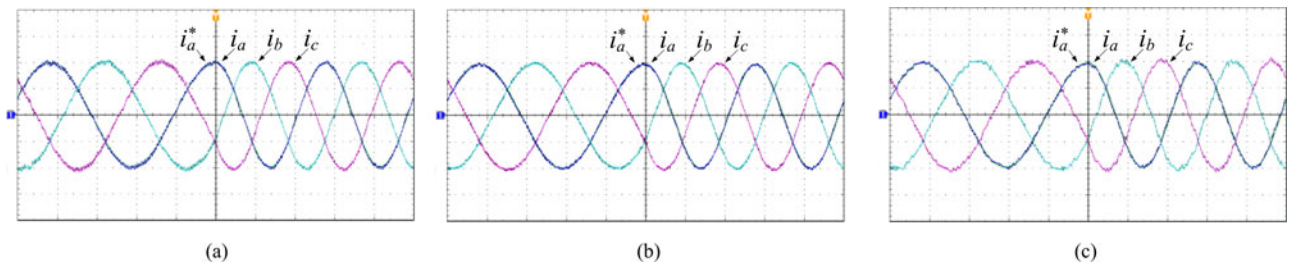

Fig. 26. Experimental waveforms of the three-phase load currents (i_a, i_b, and i_c) and a-phase reference current (i_a^*) (3 A/div and 4 ms/div) a frequency step change from 60 to 90 Hz for (a) the proposed RCMV-MPC method I, (b) the proposed RCMV-MPC method II, and (c) the conventional method ($T_s = 100$ μs and $V_{\rm dc} = 100$ V).

The dynamic responses for the sampling time $T_s = 100$ μs are shown in Figs. 15 and 16. The reference current has a step change in the frequency from 60 to 90 Hz in Fig. 15, whereas the magnitude of the reference currents is subject to a half-step change in Fig. 16. It is readily observed that the three-phase load currents controlled by the two proposed RCMV-MPC schemes follow the reference change as fast as those controlled by the conventional method for both step changes.

V. Experimental Results

The two proposed RCMV-MPC methods were tested using a prototype setup, where the entire switching algorithms with the current control methods were implemented in a DSP board (TMS320F28335) to generate sinusoidal load currents with a 60-Hz fundamental output frequency. Figs. 17 and 18 show the experimental waveforms obtained from the RCMV-MPC methods I and II with $T_s = 100$ μs, $I^* = 6$ A, and $V_{\rm dc} = 100$ V.

For comparison, the VSI based on the conventional model predictive control method is operated under the same operating conditions, and the resulting waveforms are shown in Fig. 19. Figs. 17 and 18 show that the experimental waveforms obtained from the two proposed methods are similar to those in the simulation results in Figs. 11 and 12, respectively. For the two proposed RCMV-MPC methods, the load currents controlled by the proposed methods accurately track the current reference, where the common-mode voltage $v_{\rm cm}$ is small and limited to $\pm V_{\rm dc}/6$ owing to the nonutilization of the zero vectors. Note that the common-mode voltage of the conventional method varies from $V_{\rm dc}/6$ to $-V_{\rm dc}/2$, as shown in Fig. 19(b), because only $\mathbf{V}_0$ is used in the control algorithm. The output voltages of the VSI operated by the proposed RCMV-MPC methods I and II in Figs. 17(b) and 18(b) are different from the voltage of the conventional method in Fig. 19(b) depending on the utilization of the zero vectors. In addition, the ripple components of the load currents in the proposed RCMV-MPC method I are almost similar to those observed in the conventional model predictive method, whereas the proposed RCMV-MPC method II results in reduced ripples of the load currents than the conventional method. The frequency spectra of the load currents obtained from the proposed and conventional methods are shown in Figs. 17(c), 18(c), and 19(c), illustrating that the proposed methods I and II result in a slightly higher THD and significantly lower THD than the conventional method, respectively. Note that the THD values in the experimental study are obtained by measuring the experimental load currents and by computing them using the power analysis application module in the Tektronix digital oscilloscope (500 MHz MSO3054). The power analysis module was set up to consider the 400th-harmonic component because it was the maximum number of harmonics to be considered by the power analysis application module.

Fig. 20 shows the experimental waveforms obtained from the proposed RCMV-MPC and conventional methods with $T_s = 200\ \mu$s. It is observed that the results are similar to those with $T_s = 100\ \mu$s, except for the increased current ripples and THD.

The effects of inductance and resistance errors used in the control models of the proposed and conventional methods are experimentally compared in Figs. 21–24. Fig. 21 shows experimental waveforms of the conventional and proposed methods, where the control algorithms are operated with the 50% underestimated inductance and exact resistance. As shown in Fig. 21, the load currents of both the proposed and conventional methods exhibit increased ripples and deviations from the references. In addition, the waveforms resulting from the control methods with the 50% overestimated inductance and correct resistance are shown in Fig. 22. The current waveforms with the overestimated inductances in both the proposed and conventional controllers in Fig. 22 are less deteriorated than those with the underestimated inductance in Fig. 21. Furthermore, Figs. 23 and Fig. 24 show the experimental results of the proposed RCMV-MPC methods with the 50% underestimated and 50% overestimated resistance as well as the exact inductance, respectively. It is observed that the current waveforms obtained from the proposed methods are relatively unaffected by the inaccurate resistance value. Thus, the THD and current errors are more affected by the load inductance than by the load resistance in the proposed RCMV-MPC methods, as in the conventional scheme.

The dynamic responses of the proposed and conventional methods with the sampling time $T_s = 100\ \mu$s are shown in Figs. 25 and 26. For the proposed RCMV-MPC methods, the three-phase load currents follow the change in the reference with fast dynamics as observed in the conventional method for step changes in both frequency and magnitude. In the experimental setup, the execution time required to complete the entire algorithms of the proposed RCMV-MPC methods I, II, and the conventional method were calculated by measuring calculation cycles of the DSP board. The total execution time of the proposed methods I and II in the experimental study were 19.83 and 47.01 μs, respectively. As a result, it is concluded that the proposed method II results in better performance in the current errors and the THD values at the expense of the higher number of switching and the higher complexity of calculation than the proposed method I.

VI. Conclusion

This paper has proposed the RCMV-MPC methods to reduce the common-mode voltage of three-phase VSIs as well as to control the load currents with fast dynamics. In the proposed RCMV-MPC methods, only nonzero vectors are utilized to reduce the common-mode voltage by avoiding the zero vectors that generate the highest common-mode voltages. In addition, two nonzero voltage vectors are selected and applied in one sampling period to compensate for the reduced number of usable voltage states. The two selected nonzero vectors are distributed in one sampling period in such a way as to minimize the error between the reference and actual load currents. On the basis of the two nonzero vectors and their optimal distribution in one sampling period, the proposed RCMV-MPC methods can reduce the common-mode voltage as well as control the load currents with fast transient response and satisfactory load current ripple performance compared with the conventional model predictive control method.

References

[1] M. P. Kazmierkowski, R. Krishnan, and F. Blaabjerg, *Control in Power Electronics*. New York, NY, USA: Academic, 2002.

[2] N. Mohan, T. M. Underland, and W. P. Robbins, *Power Electronics*, 2nd ed. New York, NY, USA: Wiley, 1995.

[3] A. Ajami, M. Oskuee, A. Mokhberdoran, and M. Khosroshahi, "Advanced cascade multilevel converter with reduction in number of components," *J. Elect. Eng. Technol.*, vol. 9, no. 1, pp. 127–135, 2014.

[4] S. Sinthusonthishat and N. Chuladaycha, "A simplified modulation strategy for three-leg voltage source inverter fed unsymmetrical two-winding induction motor," *J. Elect. Eng. Technol.*, vol. 8, no. 6, pp. 1337–1334, 2013.

[5] J. Gholinezhad and R. Noroozian, "Analysis of cascaded H-bridge multilevel inverter in DTC-SVM induction motor drive for FCEV," *J. Elect. Eng. Technol.*, vol. 8, no. 2, pp. 304–315, 2013.

[6] G. Park, S. Lee, S. Jin, and S. Kwak, "Integrated modeling and analysis of dynamics for electric vehicle powertrains," *Expert Syst. Appl.*, vol. 41, no. 5, pp. 2595–2607, Apr. 2014.

[7] S. Kwak, "Pulse-driven LED circuit with transformer based current balance technique," *Int. J. Electron.*, vol. 101, no. 12, pp. 1683–1693, Dec. 2014.

[8] Y. Atia and M. Salem, "Microcontroller-based improved predictive current controlled VSI for single-phase grid-connected systems," *J. Power Electron.*, vol. 13, no. 6, pp. 1016–1023, Nov. 2013.
[9] M. Duran, J. A. Riveros, F. Barrero, H. Guzman, and J. Prieto, "Reduction of common-mode voltage in five-phase induction motor drives using predictive control techniques," *IEEE Trans. Ind. Appl.*, vol. 48, no. 6, pp. 2059–2067, Nov. 2012.
[10] J. W. Kimball and M. Zawodniok, "Reducing common-mode voltage in three-phase sine-triangle PWM with interleaved carriers," *IEEE Trans. Power Electron.*, vol. 26, no. 8, pp. 2229–2236, Aug. 2011.
[11] S. Lakshminarayanan, G. Monsai, P. N. Tekwani, K. K. Mohapatra, and K. Gopakumar, "Twelve-sided polygonal voltage space vector based multilevel inverter for an induction motor drive with common-mode voltage elimination," *IEEE Trans. Ind. Electron.*, vol. 54, no. 5, pp. 2761–2768, Oct. 2007.
[12] S. Kouro, P. Cortes, R. Vargas, U. Ammann, and J. Rodriguez, "Model predictive control—A simple and powerful method to control power converters," *IEEE Trans. Ind. Electron.*, vol. 56, no. 6, pp. 1826–1838, Jun. 2009.
[13] J. Rodrguez, J. Pontt, C. Silva, P. Correa, P. Lezana, P. Cortés, and U. Ammann, "Predictive current control of a voltage source inverter," *IEEE Trans. Ind. Electron.*, vol. 54, no. 1, pp. 495–503, Feb. 2007.
[14] R. Vargas, P. Cortes, U. Ammann, J. Rodriguez, and J. Pontt, "Predictive control of a three-phase neutral-point-clamped inverter," *IEEE Trans. Ind. Electron.*, vol. 54, no. 5, pp. 2697–2705, Oct. 2007.
[15] P. Cortes, J. Rodriguez, P. Antoniewicz, and M. Kazmierkowski, "Direct power control of an AFE using predictive control," *IEEE Trans. Power Electron.*, vol. 23, no. 5, pp. 2516–2523, Sep. 2008.
[16] V. Yaramasu, M. Rivera, Bin Wu, and J. Rodriguez, "Model predictive current control of two-level four-leg inverters—Part I: Concept, algorithm, and simulation analysis," *IEEE Trans. Power Electron.*, vol. 28, no. 7, pp. 3459–3468, Jul. 2013.
[17] C. D. Townsend, T. J. Summers, J. Vodden, A. J. Watson, R. E. Betz, and J. C. Clare, "Optimization of switching losses and capacitor voltage ripple using model predictive control of a cascaded H-bridge multilevel statcom," *IEEE Trans. Power Electron.*, vol. 28, no. 7, pp. 3077–3087, Jul. 2013.
[18] R. Vargas, U. Ammann, B. Hudoffsky, J. Rodriguez, and P. Wheeler, "Predictive torque control of an induction machine fed by a matrix converter with reactive input power control," *IEEE Trans. Power Electron.*, vol. 25, no. 6, pp. 1426–1438, Jun. 2010.
[19] P. Cortes, J. Rodriguez, C. Silva, and A. Flores, "Delay compensation in model predictive current control of a three-phase inverter," *IEEE Trans. Ind. Electron.*, vol. 59, no. 2, pp. 1323–1325, Feb. 2012.
[20] J. Rodriguez, M. P. Kazmierkowski, J. R. Espinoza, P. Zanchetta, H. Abu-Rub, H. A. Young, and C. A. Rojas, "State of the art of finite control set model predictive control in power electronics," *IEEE Trans. Ind. Informat.*, vol. 9, no. 2, pp. 1003–1016, May 2013.
[21] J. Barros, J. Silva, and E. Jesus, "Fast-predictive optimal control of NPC multilevel converters," *IEEE Trans. Ind. Electon.*, vol. 60, no. 2, pp. 619–627, Feb. 2013.
[22] Y. Han and L. Xu, "Design and implementation of a robust predictive control scheme for active power filters," *J. Power Electron.*, vol. 11, no. 5, pp. 751–758, Nov. 2011.
[23] S. Kwak and J. Park, "Switching strategy based on model predictive control of VSI to obtain high efficiency and balanced loss distribution," *IEEE Trans. Power Electron.*, vol. 29, no. 9, pp. 4551–4567, Sep. 2014.
[24] J. Hu and Z. Q. Zhu, "Improved voltage-vector sequences on dead-beat predictive direct power control of reversible three-phase grid-connected voltage-source converters," *IEEE Trans. Power Electron.*, vol. 28, no. 1, pp. 254–267, Jan. 2013.
[25] S. Kwak, U. Moon, and J. Park, "Predictive-control-based direct power control with an adaptive parameter identification technique for improved AFE performance," *IEEE Trans. Power Electron.*, vol. 29, no. 11, pp. 6178–6187, Nov. 2014.
[26] Z. Boulghasoul, L. El Bahir, A. Elbacha, and E. Elwarraki, "Adaptive-predictive controller based on continuous-time poisson-laguerre models for induction motor speed control improvement," *J. Elect. Eng. Technol.*, vol. 9, no. 3, pp. 908–925, 2014.
[27] M. Cacciato, A. Consoli, G. Scarcella, G. Scelba, and A. Testa, "A novel space-vector modulation technique for common mode emissions reduction," in *Proc. Int. Conf. Elect. Mach. Power Electron.*, 2007, pp. 199–204.

Sangshin Kwak (S'02–M'05) received the Ph.D. degree in electrical engineering from Texas A&M University, College Station, TX, USA, in 2005.

From 1999 to 2000, he was a Research Engineer at LG Electronics, Changwon, Korea. He was also with Whirlpool R&D Center, Benton Harbor, MI, USA, in 2004. From 2005 to 2007, he was a Senior Engineer in Samsung SDI R&D Center, Yongin, Korea. From 2007 to 2010, he was an Assistant Professor at Daegu University, Gyeongsan, Korea. Since 2010, he has been with Chung-ang University, Seoul, Korea, currently as an Associate Professor. His research interests include topology design, modeling, control, and analysis of ac/dc, dc/ac, ac/ac power converters including resonant converters for adjustable speed drives and digital display drivers as well as modern control theory applied to DSP-based power electronics.

Sung-ki Mun received the B. S. degree in electrical and electronics engineering from Chung-ang University, Seoul, Korea, in 2014. He is currently working toward the M.S. degree in electrical and electronics engineering from Chung-ang University.

His research interests include control and analysis for multilevel inverters and voltage source inverters.